Bi-level Multi-objective Joint Planning of Distribution Networks Considering Uncertainties

Shouxiang Wang, Yichao Dong, Qianyu Zhao, and Xu Zhang

***Abstract*—With the increasing penetration of photovoltaics in distribution networks, the adaptability of distribution network under uncertainties needs to be considered in the planning of distribution systems. In this paper, the interval arithmetic and affine arithmetic are applied to deal with uncertainties, and an affine arithmetic based bi-level multi-objective joint planning model is built, which can obtain the planning schemes with low constraint-violation risk, high reliability and strong adaptability. On this basis, a bi-level multi-objective solution methodology using affine arithmetic based non-dominated sorting genetic algorithm II is proposed, and the planning schemes that simultaneously meet economy and adaptability goals under uncertainties can be obtained. To further eliminate bad solutions and improve the solution qualities, an affine arithmetic based dominance relation weakening criterion and a deviation distance based modification method are proposed. A 24-bus test system and a 10 kV distribution system of China are used for case studies. Different uncertainty levels are compared, and a sensitivity analysis of key parameters is conducted to explore their impacts on the final planning schemes. The simulation results verify the advantages of the proposed affine arithmetic based planning method.**

***Index Terms*—Affine arithmetic, adaptability, multi-objective joint planning, Pareto optimal front, uncertainty.**

NOMENCLATURE

A. Sets

Ω_n, Ω_{ss}, Ω_l	Sets of buses, substation buses, and lines
Ω_{ssa}, Ω_{la}	Sets of candidate substation buses and candidate lines to be constructed
Ω_c, Ω_k	Sets of types of substation and conductor
Ω_h, $\Omega_{t,h}$	Sets of stages and time slots in stage h
$\Omega^d_{n,h}$, $\Omega^d_{l,h}$, $\Omega^{d,tie}_{l,h}$	Sets of all buses, lines, and tie-lines at substation d in stage h

B. Parameters

α_{loss}, α_{pro}	Network loss cost and photovoltaic (PV) generation profit per unit of electricity
α_1, α_2	Weight coefficients of tie-line connection degree and network cohesion degree
α_3, α_4	Weight coefficients of voltage violation margin and current violation margin
$\varepsilon_{t,h}$	Duration of each time slot in stage h
λ_1, λ_2	Inflation rate and interest rate
$c^{cons}_{ss,c}$, $c^{cons}_{l,k}$, c^{cons}_{PV}, c^{cons}_{SVC}	Construction costs of type-c substation, unit length conductor-k line, unit PV power, and unit static var compensator (SVC)
$c^{up}_{ss,c}$, $c^{up}_{l,k}$	Upgrade costs of type-c substation and unit length conductor-k line
$c^{o\&m}_{ss,c}$, $c^{o\&m}_{l,k}$, $c^{o\&m}_{PV}$, $c^{o\&m}_{SVC}$	Operation and maintenance costs of type-c substation, unit length conductor-k line, unit PV power, and unit SVC
$I^{\max}_{l,k}$, $S^{\max}_{l,k}$	The maximum allowable current magnitude and apparent power for conductor-k line
l_{ij}	Length of line ij
$N^{\max}_{PV}$, $N^{\max}_{SVC}$	The maximum numbers of buses with PV and SVC installations
N_{Ω_h}, $N_{\Omega_{ss}}$, $N_{\Omega^d_{n,h}}$	Sizes of sets Ω_h, Ω_{ss}, and $\Omega^d_{n,h}$
$P^{cap,\max}_{PV,i,h}$, $Q^{\max}_{SVC,i,h}$	The maximum PV installation capacity and SVC compensation capacity at bus i in stage h
$R_{i,AVG}$	Average radius of affine polynomial of the i^{th} affine objective
$S^{\max}_{ss,c}$	The maximum allowable substation capacity
$V^{\max}$	The maximum allowable voltage magnitude
$z_{l,k}$	Unit impedance of conductor-k line

C. Variables

$\sigma^{cons}_{i,c,h}$, $\delta^{cons}_{ij,k,h}$	Binary decision variables representing whether constructing type-c substation at bus i and conductor-k line ij in stage h
$\sigma^{up}_{i,c,h}$, $\delta^{up}_{ij,k,h}$	Binary decision variables representing whether upgrading type-c substation at bus i and conductor-k line ij in stage h

Manuscript received: December 30, 2020; revised: April 14, 2021; accepted: July 23, 2021. Date of CrossCheck: July 23, 2021. Date of online publication: August 27, 2021.

This work was supported in part by the National Natural Science Foundation of China (No. 52077149) and the State Grid Corporation of China Science and Technology Project (No. 5400-202199280A-0-0-00).

S. Wang, Y. Dong, and Q. Zhao (corresponding author) are with the Key Laboratory of Smart Grid of Ministry of Education, Tianjin University, Tianjin, 300072, China, and Y. Dong is also with State Grid Tianjin Electric Power Company Economic and Technological Research Institute, Tianjin 300171, China (e-mail: sxwang@tju.edu.cn; ycdong007@tju.edu.cn; zhaoqianyu@tju.edu.cn).

X. Zhang is with the State Grid Tianjin Electric Power Company, Tianjin, 300010, China (e-mail: xu.zhang3@tj.sgcc.com.cn).

DOI: 10.35833/MPCE.2020.000930

$\beta_{i,h}$, $\gamma_{i,h}$ Binary decision variables representing whether installing PV and SVC at bus i

$\tau_{i,c,h}$, $\mu_{ij,k,h}$ Binary decision variables representing whether type-c substation at bus i and conductor-k line ij are in operation

$\hat{\eta}_{PV,h}^{(t)}$ Affine PV output efficiency at time t

$\varphi_{PV,i,h}$ PV power factor at bus i in stage h

$\psi_{ij,h}$, $\psi_{ji,h}$ Binary decision variables representing whether bus i is the parent of bus j

ε^m The m^{th} noise element of affine polynomial

$c_{ij,h}$ Binary decision variable representing whether bus i and bus j are connected

$D_{tcd,h}$, $D_{ncd,h}$ Tie-line connection degree and network cohesion degree in stage h

$\hat{D}_{PV,h}^{d}$ Affine standard deviation of PV installation capacity for substation d

$d_{AVG}(x_k)$ Distance between $f_i^0(x_k)$ and $f_{i,AVG}^0$

$e_{ij,h}$ Electrical distance between buses i and j

$\hat{f}_{inv,h}$, $\hat{f}_{o\&m,h}$, $\hat{f}_{loss,h}$, $\hat{f}_{pro,h}$ Affine investment cost, operation and maintenance cost, network loss cost, and PV generation profit in stage h

$\hat{f}_i(x_k)$ The i^{th} affine objective of solution x_k

$f_i^{(0)}(x_k)$, $f_i^m(x_k)$ Central value and the m^{th} noise coefficient of $\hat{f}_i(x_k)$

$f_{i,AVG}^{(0)}$, $f_{i,AVG}$ Average central value of the i^{th} affine objective and average value of the i^{th} deterministic objective

$\hat{\boldsymbol{F}}(x_k)$, $\widehat{\boldsymbol{F}}(x_k)$ Affine and interval multi-objective vectors of solution x_k

$\hat{\boldsymbol{F}}_{AVG}$, $\widehat{\boldsymbol{F}}_{AVG}$ Affine and interval multi-objective vectors of average level

$G_{ij,pf,h}$, $B_{ij,pf,h}$ Line conductance and susceptance between phase-p of bus i and phase-f of bus j in stage h

$\hat{I}_{ij,p,k,h}^{(t)}$ Affine phase-p current magnitude of conductor-k line at time t in stage h

$L(\cdot)$, $\bigcap$ Interval length and intersection operation

N_d Number of deterministic objectives

$O_{AVG}(x_k)$ Overlapping volume between hypercubes $\widehat{\boldsymbol{F}}(x_k)$ and $\widehat{\boldsymbol{F}}_{AVG}$

$\hat{P}_{PV}^{cap}$, $\hat{Q}_{SVC}$ Affine PV installation capacity and SVC compensation capacity

$\hat{P}_{i,h}^{(t)}$, $\hat{Q}_{i,h}^{(t)}$ Affine active power and reactive power injections of bus i at time t in stage h

$\hat{P}_{PV,i,h}^{(t)}$, $\hat{Q}_{PV,i,h}^{(t)}$ Affine PV active power and reactive power of bus i at time t in stage h

$\hat{P}_{L,i,h}^{(t)}$, $\hat{Q}_{L,i,h}^{(t)}$ Affine load active power and reactive power of bus i at time t in stage h

$S_{ij,p,k}^{(t)}$ Apparent power of conductor-k at time t

$S_{ss,i,c,h}^{(t)}$ Capacity of type-c substation at time t

$\hat{V}_{i,h}^{(t)}$, $\hat{\theta}_{ij,h}^{(t)}$ Affine voltage magnitude of bus i and voltage angle difference between bus i and bus j at time t in stage h

$\hat{V}_h^{mar}$, $\hat{I}_h^{mar}$ Affine voltage violation margin and current violation margin in stage h

V_{AVG}, $V(x_k)$ Volumes of hypercubes $\widehat{\boldsymbol{F}}(x_k)$ and $\widehat{\boldsymbol{F}}_{AVG}$

I. Introduction

THE increasing penetration of photovoltaics (PVs) in distribution network (DN) has inevitably induced some operational issues such as voltage violation [1]-[3], increased thermal stress [4], and degraded power quality [5]. To solve these issues, the adaptive planning of active distribution network (ADN) has become one of the research hotspots. In the traditional DN planning model, the cost concerning investment, reliability, network loss, and grid power purchase is taken as the main objective [6]. On this basis, some improvements have been made in recent years. In [7], the DN planning problem is formulated as second-order cone programming by the linearization technique. Some researchers have focused on multistage planning considering geographical locations, environmental benefits, and multistage needs. In [8], the DN multistage planning considering different types, locations and installation cycles of DN devices is proposed to minimize the total economic cost. In [9], the linearization technique is used to build a multistage mixed-integer linear programming (MILP) model, and the total cost is minimized by voltage regulator installation and network reconfiguration.

However, the objectives of the above models are mainly economy or reliability while the PV hosting capacity is rarely considered, which will restrict the enhancement of adaptability. Therefore, a DN planning model with discrete variables and nonlinear power flow is presented in [10] to maximize the PV hosting capacity. In [11], the network reconfiguration is formulated as a nonlinear and non-differentiable optimization model for hosting capacity improvement. In [12], a two-stage planning model for adaptability enhancement is proposed, where the first stage solves static investment problem and the second stage solves operational issue. Moreover, the PV and load uncertainties have great impacts on the safe and stable operation of DN as well as DN planning schemes. Although some researchers have tried to reduce impacts of uncertainties by the artificial intelligence approaches [13], the applicability of the above deterministic methods will be limited for lacking consideration of multiple uncertainties.

Currently, the probabilistic methods, robust methods, and interval methods are the three commonly used methods for dealing with uncertainty problems. Generally, the probabilistic methods [14]-[16] describe various uncertainties depending on the probability density functions (PDFs) generated by massive scenario simulations. In [14], a stochastic planning model with techno-economic and environmental indices is built, where the intermittency of PV and load is quantified by K-means based probabilistic method. In [15], the uncertainties of heat and electricity demands as well as PV outputs are quantified by massive scenario simulations. In [16], the Latin hypercube sampling and scenario reduction tech-

niques are used to build a probabilistic planning model. Although the probabilistic methods can effectively quantify multiple uncertainties, their performances are heavily dependent on the accuracy of PDFs. In reality, it is generally intractable to obtain accurate PDFs of PVs or loads, especially with limited measurement data, which restricts the application of probabilistic methods [17].

For addressing the drawbacks of probabilistic methods in dealing with uncertainties, the robust methods and interval methods are two feasible methods. The robust methods usually characterize uncertainties through the polyhedral uncertainty sets, and the solution robustness can be effectively controlled by the budget of uncertainty [18]-[20]. However, the robust optimization model is generally a nonlinear and nonconvex min-max-min problem, which cannot be solved directly by commercial optimization packages [18]. Hence, a bi-level or tri-level decomposition strategy comprising primal and dual cuts is essential, and the convexification of power flow equation is needed to guarantee convergence [19], [20], which increases the model complexity and computational burden.

In comparison, the interval methods are more applicable in dealing with uncertainty problems because all uncertain variables are expressed by their upper and lower bounds, which are relatively easier to obtain in most cases. The superiority of interval methods becomes more obvious, especially under the environment of insufficient meter configurations [21]-[23]. Generally, the interval methods can be realized in two ways, namely interval arithmetic (IA) and affine arithmetic (AA). IA usually has the drawback of conservative computation when various uncertain variables are interrelated, which can be overcome by AA. AA can keep track on the dependencies of multiple uncertain variables and reduce the computation conservativeness by the complex operations of multiple affine polynomials. In a sense, AA is an advanced interval method with higher computation accuracy and lower conservativeness.

At present, some references [24], [25] have used IA for DN uncertainty planning, while AA has not been applied for DN planning considering uncertainties in the existing literatures. Therefore, an AA-based adaptability-oriented bi-level multi-objective joint planning model is built in this paper, and the AA-based non-dominated sorting genetic algorithm II (AA-NSGA-II) is used to calculate the AA-based Pareto optimal front (AA-POF). With an expanded analysis scope of DN adaptive planning and a comprehensive coverage on uncertainties, the proposed method can obtain more rational planning schemes with better economy and adaptability goals under uncertainties. The main contributions of this paper are as follows.

1) To realize the goal of DN adaptability enhancement, two indices, namely network structural adaptability and operational adaptability, are proposed. Meanwhile, the concept of uneven degree of PV configuration is introduced to adequately improve the PV hosting capacity through a more even PV configuration instead of the extreme one. On this basis, an adaptability-oriented bi-level multi-objective joint planning model is established, which can obtain the planning schemes with low constraint-violation risk, high reliability, and strong adaptability.

2) IA and AA are applied to precisely quantify uncertainty fluctuations of PVs and loads, and the deterministic planning model has been improved by incorporating affine parameters. On this basis, an AA-NSGA-II-based bi-level multi-objective solution methodology is proposed to calculate AA-POF. The obtained AA-POF represents a set of optimal planning schemes that can simultaneously meet the economy and adaptability goals of DN considering uncertainties, which is of great significance for practical DN planning in the complex uncertain environment.

3) To further eliminate bad solutions in AA-POF and improve the solution qualities, an AA-based dominance relation weakening criterion and a deviation-distance-based AA-POF modification method are proposed. The comparison analysis of different uncertainty levels is conducted to explore their diverse interval variations. The results of AA-based planning method are compared with IA and Monte Carlo simulation (MCS) methods to demonstrate its advantages. In addition, a sensitivity analysis is conducted to explore the impacts of key parameters on the final planning schemes.

The remaining parts of this paper are organized as follows. Section II presents the problem formulation, which establishes the AA-based bi-level multi-objective joint planning model. Section III proposes the AA-NSGA-II-based solution methodology. Section IV conducts the case study and sensitivity analysis. Finally, the main conclusions are drawn in Section V.

II. Problem Formulation

In reality, the PV power outputs are inevitably affected by various uncertain factors such as variable solar radiations and temperatures, and load demands also constantly change with weather variations and electricity price adjustment [17]. The uncertainty fluctuations of PVs and loads can directly affect the uncertain power injections of all buses and then affect the uncertain power flow of DN, which has great impacts on the safe and stable operation of DN as well as DN planning schemes. To this end, IA and AA are applied in this paper to deal with uncertainties. IA is a numerical method where all uncertain variables are expressed in interval forms with the upper and lower bounds. AA is an advanced interval method where the dependencies of uncertain variables are considered, and the computation conservativeness can be effectively reduced by the complex operations of affine polynomials. The detailed arithmetical operations of IA and AA can be found in [26]. On this basis, the AA-based adaptability-oriented bi-level multi-objective joint planning model is built as follows.

A. Objective Functions

The bi-level multi-objective joint planning model includes four objectives in total. In the upper-level model, the construction and upgrade strategy of substation and line is optimized for minimizing the total economic cost and maximizing the network structural adaptability. In the lower-level model, the configuration strategy of PV and static var compensation (SVC) is optimized for maximizing the operational adaptability and minimizing the uneven degree of PV configuration.

1) AA-based Total Economic Cost

The AA-based total economic cost $\hat{f}_1$ in (1) is defined as the weighted sum of affine net present value of investment cost, operation and maintenance cost, network loss cost, and PV generation profit formulated by (2)-(5). The objective $\hat{f}_1$ is the fundamental objective for DN multistage planning.

$$\min \hat{f}_1 = \sum_{h \in \Omega_h} \left(\frac{1+\lambda_1}{1+\lambda_2} \right)^h (f_{inv,h} + f_{o\&m,h} + f_{loss,h} - f_{pro,h}) \tag{1}$$

$$\hat{f}_{inv,h} = \sum_{i \in \Omega_{ss}} \sum_{c \in \Omega_c} (c_{ss,c}^{cons} \sigma_{i,c,h}^{cons} + c_{ss,c}^{up} \sigma_{i,c,h}^{up}) + \sum_{ij \in \Omega_l} \sum_{k \in \Omega_k} (c_{l,k}^{cons} \delta_{ij,k,h}^{cons} l_{ij} + c_{l,k}^{up} \delta_{ij,k,h}^{up} l_{ij}) + \sum_{i \in \Omega_n} c_{PV}^{cons} \beta_{i,h} \hat{P}_{PV,i,h}^{cap} + \sum_{i \in \Omega_n} c_{SVC}^{cons} \gamma_{i,h} \tag{2}$$

$$\hat{f}_{o\&m,h} = \sum_{i \in \Omega_{ss}} \sum_{c \in \Omega_c} c_{ss,c}^{o\&m} \tau_{i,c,h} + \sum_{ij \in \Omega_l} \sum_{k \in \Omega_k} c_{l,k}^{o\&m} \mu_{ij,k,h} l_{ij} + \sum_{g=1}^{h} \sum_{i \in \Omega_n} c_{PV}^{o\&m} \beta_{i,g} \hat{P}_{PV,i,g}^{cap} + \sum_{g=1}^{h} \sum_{i \in \Omega_n} c_{SVC}^{o\&m} \gamma_{i,g} \tag{3}$$

$$\hat{f}_{loss,h} = \alpha_{loss} \varepsilon_{t,h} \sum_{t \in \Omega_{t,h}} \sum_{i,j \in \Omega_n} G_{ij,h} \left((\hat{V}_{i,h}^{(t)})^2 + (\hat{V}_{j,h}^{(t)})^2 - 2 \hat{V}_{i,h}^{(t)} \hat{V}_{j,h}^{(t)} \cos \hat{\theta}_{ij,h}^{(t)} \right) \tag{4}$$

$$\hat{f}_{pro,h} = \alpha_{pro} \varepsilon_{t,h} \sum_{t \in \Omega_{t,h}} \sum_{i \in \Omega_n} \beta_{i,h} \hat{P}_{PV,i,h}^{(t)} \tag{5}$$

2) Network Structural Adaptability

The network structural adaptability f_2 in (6) is defined as the weighted sum of two indices. The first index is the tie-line connection degree (TCD) in (7), which is quantified by the distribution density of tie-lines between different power supply areas. $D_{tcd}=0$ means there is no tie-line in operation and the corresponding power supply reliability is poor. The second index is the network cohesion degree (NCD) in (8) and (9), which is quantified by the strength of network cohesion between different geographical regions. $D_{ncd}=0$ means all substations supply power in their own geographical regions without interconnection. The objective f_2 can effectively reflect the flexibility and adaptability of DN network structure, which is also important during the whole planning horizon.

$$\max f_2 = \frac{1}{N_{\Omega_h}} \sum_{h \in \Omega_h} (\alpha_1 D_{tcd,h} + \alpha_2 D_{ncd,h}) \tag{6}$$

$$D_{tcd,h} = \frac{1}{N_{\Omega_{ss}}} \sum_{d \in \Omega_{ss}} \left(\frac{\sum_{ij \in \Omega_{l,h}^{d,tie}} \mu_{ij,h}}{\sum_{ij \in \Omega_{l,h}^{d}} \mu_{ij,h}} \right) \tag{7}$$

$$D_{ncd,h} = \frac{\sum_{i,j \in \Omega_n, j \neq \Omega_n^i} \frac{1}{e_{ij,h}}}{\sum_{i,j \in \Omega_n, j \neq i} \frac{1}{e_{ij,h}}} \tag{8}$$

$$e_{ij,h} = \begin{cases} \sum_{k \in \Omega_k} \mu_{ij,k,h} z_{l,k} l_{ij} & c_{ij,h}=1 \\ \infty & c_{ij,h}=0 \end{cases} \tag{9}$$

3) AA-based Operation Adaptability

The high penetration of PVs has great impacts on the overall level of bus voltage and line current. The AA-based operational adaptability $\hat{f}_3$ in (10) is defined as the weighted sum of voltage violation margin $\hat{V}_h^{mar}$ and current violation margin $\hat{I}_h^{mar}$ formulated by (11) and (12). $\hat{f}_3$ can effectively reflect the comprehensive constraint violation risk and DN operational adaptability under uncertainties. The larger $\hat{f}_3$ is, the more abundant space for further PV installation there will be, and the DN will present larger PV hosting capacity and stronger operational adaptability accordingly.

$$\max \hat{f}_3 = \frac{1}{N_{\Omega_h}} \sum_{h \in \Omega_h} (\alpha_3 \hat{V}_h^{mar} + \alpha_4 \hat{I}_h^{mar}) \tag{10}$$

$$\hat{V}_h^{mar} = \frac{1}{N_{\Omega_{ss}} N_{\Omega_{n,h}^d}} \sum_{d \in \Omega_{ss}} \sum_{i \in \Omega_{n,h}^d} \min_{\substack{p=a,b,c \\ \forall t \in \Omega_{t,h}}} \left| \frac{V^{\max} - \hat{V}_{i,p,h}^{(t)}}{V^{\max}} \right| \tag{11}$$

$$\hat{I}_h^{mar} = \frac{1}{N_{\Omega_{ss}}} \sum_{d \in \Omega_{ss}} \min_{\substack{p=a,b,c, \forall k \in \Omega_k \\ \forall ij \in \Omega_{l,h}^d, \forall t \in \Omega_{t,h}}} \left| \frac{I_{l,k}^{\max} - \hat{I}_{ij,p,k,h}^{(t)}}{I_{l,k}^{\max}} \right| \tag{12}$$

4) AA-based PV Configuration Uneven Degree

When a centralized PV with a large capacity is installed at the most distant terminal bus, which is called the extreme PV configuration, the voltage violation is most likely to occur. In this condition, the PV configuration presents an uneven characteristic and the PV hosting capacity will be restricted. To this end, the AA-based PV configuration uneven degree $\hat{f}_4$ is defined by (13)-(15) to quantify the uneven degree of PV configuration during all planning stages considering uncertainties. By optimizing the objective $\hat{f}_4$, the PV hosting capacity can be adequately improved through a more even PV configuration instead of the extreme PV configuration.

$$\min \hat{f}_4 = \frac{1}{N_{\Omega_h} N_{\Omega_{ss}}} \sum_{h \in \Omega_h} \sum_{d \in \Omega_{ss}} \frac{\hat{D}_{PV,h}^{d}}{\hat{P}_{PV,h}^{cap,d}} \tag{13}$$

$$\hat{D}_{PV,h}^{d} = \sqrt{\frac{1}{N_{\Omega_{n,h}^d}} \sum_{i \in \Omega_{n,h}^d} \left(\beta_{i,h} \hat{P}_{PV,i,h}^{cap} - \frac{\hat{P}_{PV,h}^{cap,d}}{N_{\Omega_{n,h}^d}} \right)^2} \tag{14}$$

$$\hat{P}_{PV,h}^{cap,d} = \sum_{i \in \Omega_{n,h}^d} \beta_{i,h} \hat{P}_{PV,i,h}^{cap} \tag{15}$$

B. Constraint Conditions

1) AA-based Three-phase Power Flow Constraints

To describe the three-phase unbalance characteristics of DN and influences of various uncertain factors, the AA-based three-phase power flow is constrained by (16)-(21), where the AA-based forward-backward sweep power flow method [22] is used for analysis.

$$\hat{P}_{i,p,h}^{(t)} = \hat{V}_{i,p,h}^{(t)} \sum_{j \in \Omega_n} \sum_{f=a}^{c} (G_{ij,pf,h} \hat{V}_{j,f,h}^{(t)} \cos \hat{\theta}_{ij,pf,h}^{(t)} + B_{ij,pf,h} \hat{V}_{j,f,h}^{(t)} \sin \hat{\theta}_{ij,pf,h}^{(t)}) \tag{16}$$

$$\hat{Q}_{i,p,h}^{(t)} = \hat{V}_{i,p,h}^{(t)} \sum_{j \in \Omega_n} \sum_{f=a}^{c} (G_{ij,pf,h} \hat{V}_{j,f,h}^{(t)} \sin \hat{\theta}_{ij,pf,h}^{(t)} - B_{ij,pf,h} \hat{V}_{j,f,h}^{(t)} \cos \hat{\theta}_{ij,pf,h}^{(t)}) \tag{17}$$

$$\hat{P}_{i,p,h}^{(t)} = \beta_{i,h} \hat{P}_{PV,i,p,h}^{(t)} - \hat{P}_{L,i,p,h}^{(t)} \tag{18}$$

$$\hat{Q}_{i,p,h}^{(t)} = \beta_{i,h} \hat{Q}_{PV,i,p,h}^{(t)} + \gamma_{i,h} \hat{Q}_{SVC,i,p,h} - \hat{Q}_{L,i,p,h}^{(t)} \tag{19}$$

$$\hat{P}^{(t)}_{PV,\,i,p,h}=\hat{P}^{cap}_{PV,i,p,h}\hat{\eta}^{(t)}_{PV,h} \tag{20}$$

$$\hat{Q}^{(t)}_{PV,i,p,h}=\hat{P}^{(t)}_{PV,i,p,h}\tan(\arccos\varphi_{PV,i,h}) \tag{21}$$

2) Radial Topology Constraints

The DN radial topology should be maintained during the whole planning horizon as formulated by (22) and (23).

$$\psi_{ij,h}+\psi_{ji,h}=\mu_{ij,h}\quad \forall ij\in\Omega_l,\forall h\in\Omega_h \tag{22}$$

$$\psi_{ij,h}=0\quad \forall j\in\Omega_{ss},\forall h\in\Omega_h \tag{23}$$

$$\sum_{i\in\Omega_n}\psi_{ij,h}=1\quad \forall j\in\Omega_n\backslash\Omega_{ss},\forall h\in\Omega_h \tag{24}$$

3) AA-based Steady-state Operation Constraints

The AA-based steady-state operation constraints concerning bus voltage, line current, and apparent power should be satisfied for each time slot as formulated by (25)-(27), which can ensure the normal operation of DN under uncertainties. The PV installation capacity, SVC compensation capacity, and substation capacity also need to be constrained by (28)-(30).

$$V^{\min}\le\underline{V}^{(t)}_{i,p,h}<\bar{V}^{(t)}_{i,p,h}\le V^{\max}\quad \forall i\in\Omega_n,\forall p=a,b,c \tag{25}$$

$$\left|\bar{I}^{(t)}_{ij,p,k,h}\right|\le I^{\max}_{l,k}\quad \forall ij\in\Omega_l,\forall k\in\Omega_k,\forall p=a,b,c \tag{26}$$

$$\left|\bar{S}^{(t)}_{ij,p,k,h}\right|\le S^{\max}_{l,k}\quad \forall ij\in\Omega_l,\forall k\in\Omega_k,\forall p=a,b,c \tag{27}$$

$$\bar{P}^{cap}_{PV,i,h}\le P^{cap,\max}_{PV,i,h}\quad \forall i\in\Omega_n \tag{28}$$

$$\left|\bar{Q}_{SVC,i,h}\right|\le Q^{\max}_{SVC,i,h}\quad \forall i\in\Omega_n \tag{29}$$

$$S^{(t)}_{ss,i,c,h}\le S^{\max}_{ss,c}\quad \forall i\in\Omega_{ss},\forall c\in\Omega_c \tag{30}$$

where the horizontal lined superscript $\overline{(\cdot)}$ and subscript $\underline{(\cdot)}$ represent the upper and lower bounds of uncertain variable, respectively.

4) Multistage Planning Constraints

During the whole planning horizon, $N^{\max}_{PV}$ and $N^{\max}_{SVC}$ should be restricted by (31) and (32), respectively. Other multistage planning constraints for substations and lines are described in (33)-(36).

$$\sum_{h\in\Omega_h}\sum_{i\in\Omega_n}\beta_{i,h}\le N^{\max}_{PV} \tag{31}$$

$$\sum_{h\in\Omega_h}\sum_{i\in\Omega_n}\gamma_{i,h}\le N^{\max}_{SVC} \tag{32}$$

$$\sum_{h\in\Omega_h}\sum_{c\in\Omega_c}(\sigma^{cons}_{i,c,h}+\sigma^{up}_{i,c,h})\le 1\quad \forall i\in\Omega_{ss} \tag{33}$$

$$\sum_{h\in\Omega_h}\sum_{k\in\Omega_k}(\delta^{cons}_{ij,k,h}+\delta^{up}_{ij,k,h})\le 1\quad \forall ij\in\Omega_l \tag{34}$$

$$\tau_{i,h}=\begin{cases}\sum_{g=1}^{h}\sum_{c\in\Omega_c}\sigma^{cons}_{i,c,g} & \forall i\in\Omega_{ssa},\forall h\in\Omega_h\\ 1 & \forall i\in\Omega_{ss}\backslash\Omega_{ssa},\forall h\in\Omega_h\end{cases} \tag{35}$$

$$\mu_{ij,h}\le\sum_{g=1}^{h}\sum_{k\in\Omega_k}\delta^{cons}_{ij,k,g}\quad \forall ij\in\Omega_{la},\forall h\in\Omega_h \tag{36}$$

III. Solution Methodology

With the properties of fast non-dominated sorting and elitist strategy, NSGA-II has received a lot of attentions in solving multi-objective optimization problems [27]. By incorporating affine parameters in NSGA-II, AA-NSGA-II is proposed in [23]. In AA-NSGA-II, the objectives of all feasible solutions are compared in affine forms to reflect uncertainties. Based on AA-NSGA-II, an AA-based dominance relation weakening criterion and a deviation distance based AA-POF modification method are presented in this section, which can effectively eliminate bad solutions in the AA-POF and improve the solution qualities. On this basis, an AA-NSGA-II-based bi-level multi-objective solution methodology is proposed.

A. AA-NSGA-II Improvement

1) AA-based Dominance Relation and AA-POF

The comparison of affine variables is usually conducted based on the confidence level. The detailed calculation method of confidence level can be found in [23]. On this basis, the AA-based dominance relations between all feasible solutions in the solution space $S=\{x_k|k=1,2,\ldots,K\}$ can be determined. For an N-dimensional multi-objective minimization problem, the solution x_i dominates x_j in S if:

$$\begin{cases}\Phi\left\{\hat{f}_a(x_i)<\hat{f}_a(x_j)\right\}\ge 0.5 & \forall a\in\{1,2,\ldots,N\}\\ \Phi\left\{\hat{f}_b(x_i)<\hat{f}_b(x_j)\right\}>0.5 & \exists b\in\{1,2,\ldots,N\}\end{cases} \tag{37}$$

When no other solutions in S dominate x_k, x_k becomes an AA-based Pareto optimal solution. Thus, the set of Pareto optimal solutions containing K_{nd} solutions can be defined as $P_{nd}=\{x_k|k=1,2,\ldots,K_{nd}\}$. On this basis, the AA-POF is defined as the affine multi-objective vector of all AA-based Pareto optimal solutions as shown in (38).

$$\boldsymbol{AA\text{-}POF}=\left\{\hat{\boldsymbol{F}}(x_k)=[\hat{f}_1(x_k),\hat{f}_2(x_k),\ldots,\hat{f}_N(x_k)]^{\mathrm{T}}\,\middle|\,x_k\in P_{nd}\right\} \tag{38}$$

With the increase of N, the dimension of AA-POF will get larger accordingly. When $N=2$, the AA-POF is a set of rectangles. When $N=3$, the AA-POF is a set of cubes. When $N\ge 4$, the AA-POF will become a set of hypercubes.

2) AA-based Dominance Relation Weakening Criterion

When N is large, there will be some bad solutions in the AA-POF which only have one non-dominated objective, while other objectives are all dominated by other solutions. These bad solutions will become less feasible with the increase of N because their ratios of non-dominated objective are getting lower, which makes their infeasibility closer to those solutions without any non-dominated objective. In this case, the strict dominance relation criterion in (37) seems less applicable, and it is necessary to eliminate bad solutions by appropriately weakening the dominance relation. To this end, an AA-based dominance relation weakening criterion is proposed in this paper. Under this criterion, the solution x_i dominates x_j if:

$$\begin{cases}\Phi\left\{\hat{f}_a(x_i)<\hat{f}_a(x_j)\right\}\ge 0.5 & \forall a\le N-\left[\log_2(N-2)\right]\\ \Phi\left\{\hat{f}_b(x_i)<\hat{f}_b(x_j)\right\}<0.5 & \exists b>N-\left[\log_2(N-2)\right]\end{cases} \tag{39}$$

where $[\cdot]$ is the rounding operation.

3) Deviation Distance Based AA-POF Modification

After adopting the AA-based dominance relation weakening criterion, there may still exist bad solutions with certain objectives deviated far from the average level. These solutions are also infeasible and should be eliminated although

they are non-dominated. To this end, a deviation distance based AA-POF modification method is proposed in this paper. If the affine objectives of all Pareto optimal solutions are denoted as (40), the average central value $f_{i,AVG}^{0}$ can be calculated by (41).

$$\hat{f}_i(x_k)=f_i^{(0)}(x_k)+\sum_{m=1}^{M}f_i^m(x_k)\varepsilon^m \quad \forall x_k\in P_{nd}, i=1,2,\ldots,N \tag{40}$$

$$f_{i,AVG}^{(0)}=\frac{1}{K_{nd}}\sum_{x_k\in P_{nd}}f_i^{(0)}(x_k) \quad i=1,2,\ldots,N \tag{41}$$

On this basis, the deviation distance $D_{AVG}(x_k)$ between $\hat{\boldsymbol{F}}(x_k)$ and average level $\hat{\boldsymbol{F}}_{AVG}=[\hat{f}_{1,AVG},\hat{f}_{2,AVG},\ldots,\hat{f}_{N,AVG}]^{\mathrm{T}}$ is calculated by (42)-(46).

$$D_{AVG}(x_k)=\frac{d_{AVG}(x_k)}{O_{AVG}(x_k)+V_{AVG}+V(x_k)+1} \quad \forall x_k\in P_{nd} \tag{42}$$

$$d_{AVG}(x_k)=\sum_{i=1}^{N}\left|f_i^{(0)}(x_k)-f_{i,AVG}^{(0)}\right| \quad \forall x_k\in P_{nd} \tag{43}$$

$$O_{AVG}(x_k)=\prod_{i=1}^{N}L\left(\hat{f}_i(x_k)\cap\hat{f}_{i,AVG}\right) \quad \forall x_k\in P_{nd} \tag{44}$$

$$V_{AVG}=\prod_{i=1}^{N}\left(\frac{2}{K_{nd}}\sum_{x_k\in P_{nd}}\sum_{m=1}^{M}\left|f_i^m(x_k)\right|\right) \tag{45}$$

$$V(x_k)=\prod_{i=1}^{N}\left(2\sum_{m=1}^{M}\left|f_i^m(x_k)\right|\right) \quad \forall x_k\in P_{nd} \tag{46}$$

where the hypercubes $\widehat{\boldsymbol{F}}(x_k)$ and $\widehat{\boldsymbol{F}}_{AVG}$ can be derived from the affine polynomials of $\hat{\boldsymbol{F}}(x_k)$ and $\hat{\boldsymbol{F}}_{AVG}$ according to (47) and (48), respectively.

$$\hat{f}_i(x_k)=\left[f_i^{(0)}(x_k)-\sum_{m=1}^{M}\left|f_i^m(x_k)\right|,f_i^{(0)}(x_k)+\sum_{m=1}^{M}\left|f_i^m(x_k)\right|\right] \tag{47}$$

$$\begin{cases}\hat{f}_{i,AVG}=[f_{i,AVG}^{(0)}-R_{i,AVG},f_{i,AVG}^{(0)}+R_{i,AVG}]\\ R_{i,AVG}=\dfrac{1}{K_{nd}}\displaystyle\sum_{x_k\in P_{nd}}\sum_{m=1}^{M}\left|f_i^m(x_k)\right|\end{cases} \tag{48}$$

By comparing the deviation distances of all Pareto optimal solutions, i.e., $D_{AVG}(x_k)$ ($\forall x_k\in P_{nd}$) with the predefined maximum allowable deviation distance $D_{\max}$, the bad solutions in AA-POF can be effectively eliminated.

The deviation distance $D_{AVG}(x_k)$ only considers the affine objectives but ignores the deterministic objectives. To this end, the comprehensive deviation distance $\tilde{D}_{AVG}(x_k)$ considering all affine objectives and deterministic objectives is defined as:

$$\tilde{D}_{AVG}(x_k)=D_{AVG}(x_k)\cdot\exp\left(\sum_{i=1}^{N_d}\left|\frac{f_i(x_k)}{f_{i,AVG}}-1\right|\right) \quad \forall x_k\in P_{nd} \tag{49}$$

$$f_{i,AVG}=\frac{1}{K_{nd}}\sum_{x_k\in P_{nd}}f_i(x_k) \tag{50}$$

B. AA-NSGA-II-based Bi-level Solution Methodology

By applying the basic theories of AA-NSGA II, AA-based dominance relation weakening criterion and deviation distance-based AA-POF modification method, an AA-NSGA-II-based bi-level multi-objective solution methodology is proposed. Through the joint optimization of bi-level model, the multi-objective planning problem can be solved more effectively. The main solution flowchart is depicted in Fig. 1, and the detailed solution procedure is introduced as follows.

Step 1: initialize the chromosome codes at the upper level for construction and upgrade the strategy of substation and line, and filtrate them by (22)-(24) and (33)-(36). Then, a total of N_P^{up} feasible individuals are generated, and the population $\boldsymbol{P}^{up}$ only containing upper-level codes is formed.

Step 2: select the i^{th} individual of $\boldsymbol{P}^{up}$, i.e., I_i^{up} for replicating, and keep their upper-level codes consistent. Then, initialize the lower-level codes for configuration strategy of PV and SVC, and filtrate them by (16)-(21) and (25)-(32). A total of N_P^{down} individuals are generated and the population $\boldsymbol{P}_1(I_i^{up})$ containing upper- and lower-level codes is constituted.

Step 3: calculate the lower-level objectives $\hat{f}_3$ and $\hat{f}_4$ for each individual of $\boldsymbol{P}_1(I_i^{up})$. Then, analyze the dominance relations of $\hat{f}_3$ and $\hat{f}_4$ between different individuals by (41). Thus, the set of AA-based non-dominated solutions corresponding to $\boldsymbol{P}_1(I_i^{up})$, i.e., $\boldsymbol{F}_1^{opt}(I_i^{up})$, is determined.

Step 4: conduct the selection, crossover and mutation operations for $\boldsymbol{P}_1(I_i^{up})$ (only for the lower-level codes) to form $\boldsymbol{P}_2(I_i^{up})$, and $\boldsymbol{F}_2^{opt}(I_i^{up})$ is ascertained. After $N_{\max}$ iterations, the set of non-dominated solutions corresponding to I_i^{up}, i.e., $\boldsymbol{F}_N^{opt}(I_i^{up})$ is obtained. Then, calculate the upper-level objectives $\hat{f}_1$, f_2, and analyze the AA-based weakening dominance relations of all objectives to determine the AA-POF $\boldsymbol{F}^{opt}(I_i^{up})$.

Step 5: repeat *Steps 1-4* for all individuals of $\boldsymbol{P}^{up}$ and form $\boldsymbol{P}^{full}$ containing all sets of non-dominated solutions, where $\boldsymbol{P}^{full}=\{\boldsymbol{F}^{opt}(I_i^{up})|i=1,2,\ldots,N_P^{up}\}$. Then, analyze the AA-based weakening dominance relations of all objectives and obtain AA-POF $\boldsymbol{F}^{opt}(\boldsymbol{P}^{full})$. The final AA-POF $\boldsymbol{F}_{final}^{opt}$ can be determined by the deviation distance based modification.

IV. Case Study

A. Case Description and Parameter Setting

To verify effectiveness of the proposed method, a modified 24-bus test system [8] shown in Fig. 2 is used to conduct case study. This is a 20 kV distribution system consisting of 4 substation buses, 20 load buses, and 33 lines (including 9 tie-lines marked in red). The whole system is divided into four geographical regions, namely Z_1 - Z_4. The reference voltage is set as 1.00 p.u.. $V^{\max}$ and $V^{\min}$ are set as 1.05 p.u. and 0.95 p.u., respectively. All buses are assumed as *PQ*-type bus.

The planning horizon is divided into 3 stages, each lasting for 5 years. The data of line and peak load (power factor equals 0.9) are derived from [8] and [9], respectively. The interval construction of PV outputs and load demands with reference to [17] is depicted in Fig. 3. There are three available types of substations and conductors, and the existing substations and conductors are all type one. The data of substations and conductors are shown in Table I and Table II, respectively. The economic parameters are given in Table III. α_1, α_2, α_3 and α_4 are set as 0.5, 0.5, 0.8, and 0.2, respectively. The crossover rate and mutation rate are set as 0.5 and 0.1, respectively. In addition, all SVCs are assumed in inductive compensations. $N_{PV}^{\max}$ and $N_{SVC}^{\max}$ are both set as the total number of buses. $P_{PV,i,h}^{cap,\max}$ and $Q_{SVC,i,h}^{\max}$ are set as 1 MW and 500 kvar, respectively.

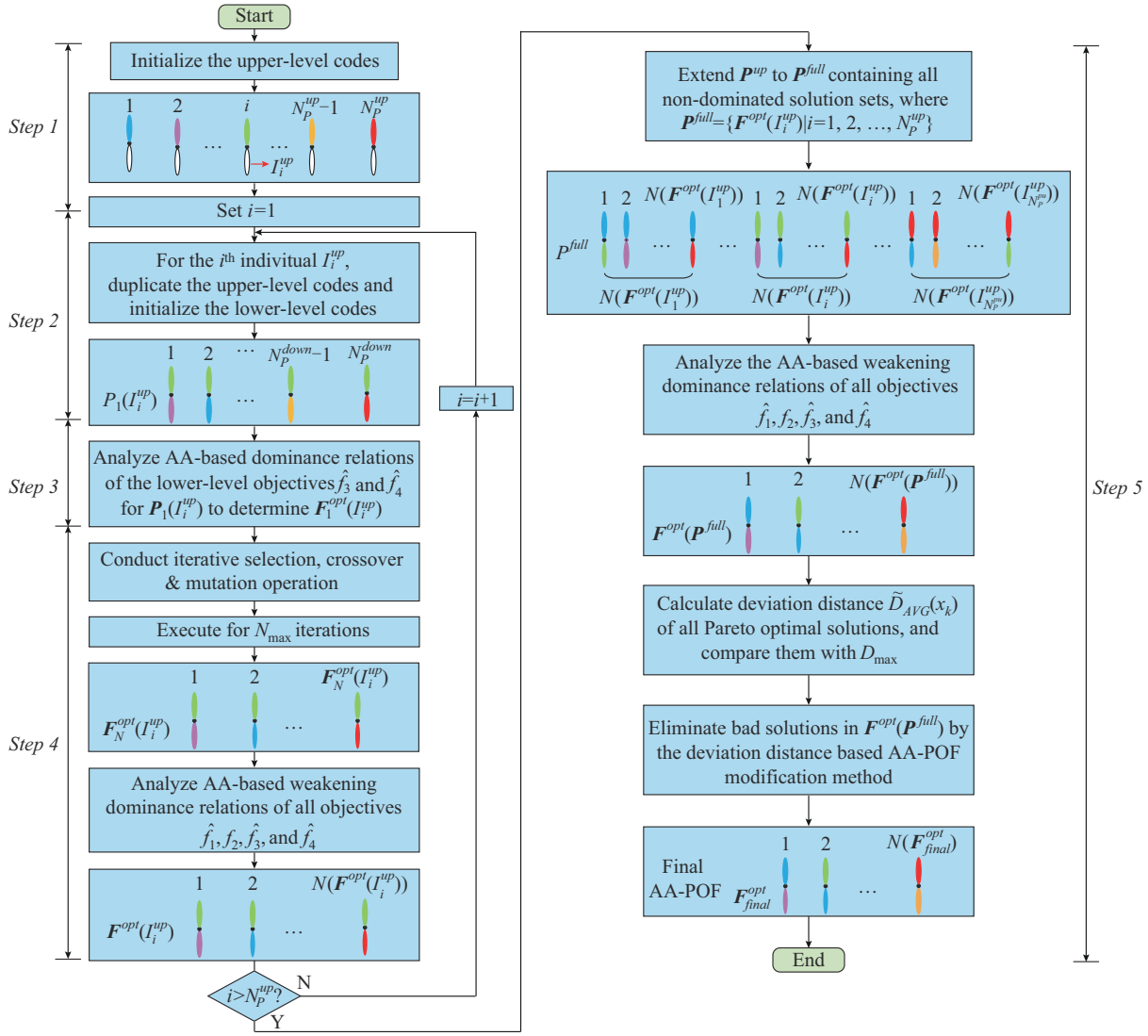

Fig. 1. Main solution flowchart.

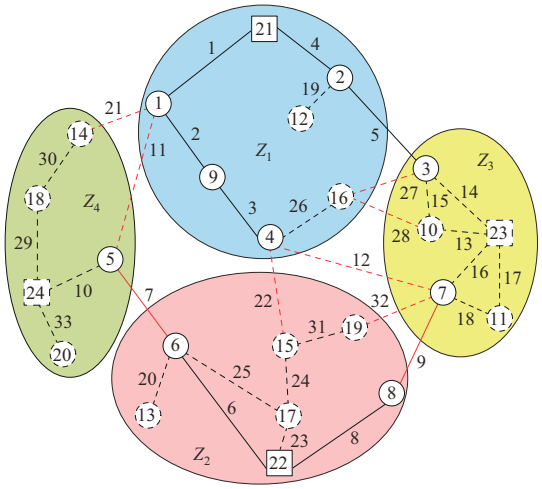

Fig. 2. Initial topology of modified 24-bus test system.

All simulation tests are implemented in C++ environment on a Dell laptop with Intel Core i7-7700HQ CPU running at 2.80 GHz with 8 GB RAM.

B. Simulation Analysis

1) AA-based Pareto Optimal Solutions

By using the bi-level multi-objective solution methodology, a total of ten Pareto optimal solutions are obtained. The planning schemes of Pareto optimal solutions No. 2 and No. 8 are shown in Fig. 4, and the interval objective values of all Pareto optimal solutions are listed in Table IV and Table V.

In Fig. 4, the letters C and U represent the lines to be constructed and upgraded, respectively. The letter T represents the substations to be constructed or upgraded. The numbers 1, 2 or 3 in bracket represent the corresponding type.

It can be observed that with the increase of total PV installation capacity, the investment cost, operation and maintenance cost as well as PV generation profit will rise up accordingly, while the network loss cost decreases in general. The solution No. 3 has larger PV capacity but lower total cost compared with solution No. 4, which means an adequate PV capacity can reduce the total cost. For the solutions with similar PV capacity, the PV configuration seems important.

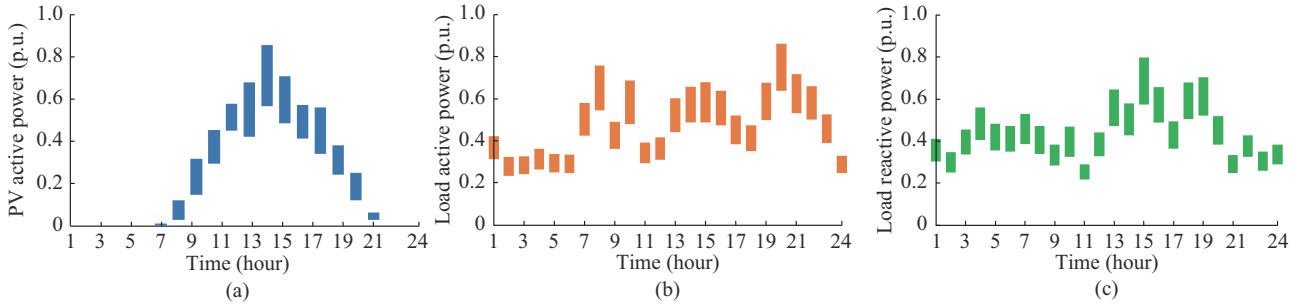

Fig. 3. Interval construction. (a) PV active power. (b) Load active power. (c) Load reactive power.

TABLE I
DATA OF DIFFERENT TYPES OF SUBSTATIONS

Ω_c	$S_{ss,c}^{\max}$ (kVA)	$c_{ss,c}^{cons}$ (k$)	$c_{ss,c}^{up}$ (k$)	$c_{ss,c}^{o\&m}$ (k$/a)
1	12000	750		2.0
2	15000	950	720	3.0
3	20000	1350	1020	4.5

TABLE II
DATA OF DIFFERENT TYPES OF CONDUCTORS

Ω_k	$z_{l,k}$ (Ω/km)	$S_{l,k}^{\max}$ (kVA)	$I_{l,k}^{\max}$ (A)	$c_{l,k}^{cons}$ ($/km)	$c_{l,k}^{up}$ ($/km)	$c_{l,k}^{o\&m}$ ($/(km·a))
1	1.268+j0.422	2260	136	10000		25
2	0.576+j0.393	4350	261	15000	11400	35
3	0.215+j0.334	9210	445	23000	17480	50

TABLE III
DATA OF NECESSARY ECONOMIC PARAMETERS

c_{PV}^{cons} ($/kW)	c_{SVC}^{cons} ($)	$c_{PV}^{o\&m}$ ($/kW·a)	$c_{SVC}^{o\&m}$ ($/a)	α_{loss} ($/kWh)	α_{pro} ($/kWh)	λ_1	λ_2
1000	3000	50	100	0.08	0.06	0.03	0.10

Specifically, a more even PV configuration, i.e., a lower PV configuration uneven degree can lead to a better power flow distribution, which is beneficial for reducing network loss and constraint violation risk. In this case, the voltage and current violation margin is increased, and the DN operational adaptability and PV hosting capacity can be effectively improved.

Meanwhile, each planning scheme corresponds to a certain network structural adaptability. The solutions No. 4, No. 8, and No. 10 have more tie-lines in operation and tighter interconnections between geographical regions, so their power supply reliability and adaptability are stronger. The index of network structural adaptability is equally important for DN planning, so these three solutions may be feasible in practice although most of their objectives are not optimal.

In addition, the variation amplitude of current violation margin is much larger than that of voltage violation margin. This is because the 24-bus system is of small scale and power supply radius, which makes the voltage rise less obvious. In this case, the DN operational adaptability is mainly dependent on current violation margin, and the ratio of α_3 and α_4 can be set smaller. With the increase of network scale and power supply radius, the variation of voltage violation margin will be more obvious. Especially in the rural DN with long lines, the voltage violation risk is much higher, and the DN operational adaptability is mainly determined by voltage violation margin, which means the ratio of α_3 and α_4 should be enlarged.

2) AA-POF Analysis

The AA-POF is depicted as a set of cubes (the length, width and height correspond to $\hat{f}_3$, $\hat{f}_4$, and $\hat{f}_1$ in order, respectively) with the mass f_2 in the multi-dimensional objective space, as shown in Fig. 5. To compare different objective values more intuitively, the projections of AA-POF on $\hat{f}_3$-$\hat{f}_4$ plane, $\hat{f}_3$-$\hat{f}_1$ plane, and $\hat{f}_4$-$\hat{f}_1$ plane are depicted in Fig. 6(a), (b), and (c), respectively.

Following the AA-based dominance relation weakening criterion, all of the ten Pareto optimal solutions obtained have two non-dominated objectives. For instance, the solution No. 6 of Fig. 6(a) has better $\hat{f}_3$ and $\hat{f}_4$ values in the two-dimensional objective space, while its $\hat{f}_1$ and f_2 values are both dominated by other solutions in region A. Meanwhile, solution No. 7 of Fig. 6(b) has better $\hat{f}_1$ and $\hat{f}_3$ values while its f_2 and $\hat{f}_4$ values are both dominated by other solutions in region B. All other solutions also show the multi-objective mutual dominance characteristics. The final Pareto optimal solutions to be adopted in practice should be selected by the DN planners based on the specific demand of each objective.

3) Deviation Distance Analysis

The deviation distances of all Pareto optimal solutions from the average level are calculated, as shown in Table VI. When only considering affine objectives $\hat{f}_1$, $\hat{f}_3$, and $\hat{f}_4$, solutions No. 6 and No. 7 have greater deviation distances compared with other solutions.

If the maximum allowable deviation distance $D_{\max}$ is set as 3.5, solutions No. 6 and No. 7 can be regarded as bad solutions and should be eliminated from the AA-POF. When further considering the deterministic objective f_2, the comprehensive deviation distance $\tilde{D}_{AVG}(x_k)$ can be calculated by (51) and (52), which is compared with $D_{AVG}(x_k)$ as shown in Fig. 7.

After considering the objective f_2, the comprehensive deviation distances of solutions No. 6 and No. 8 are enlarged more obviously, because their f_2 values are farther from the average level. At this time, only the solutions No. 6 and No. 7 have $\tilde{D}_{AVG}(x_k)$ values greater than 4.

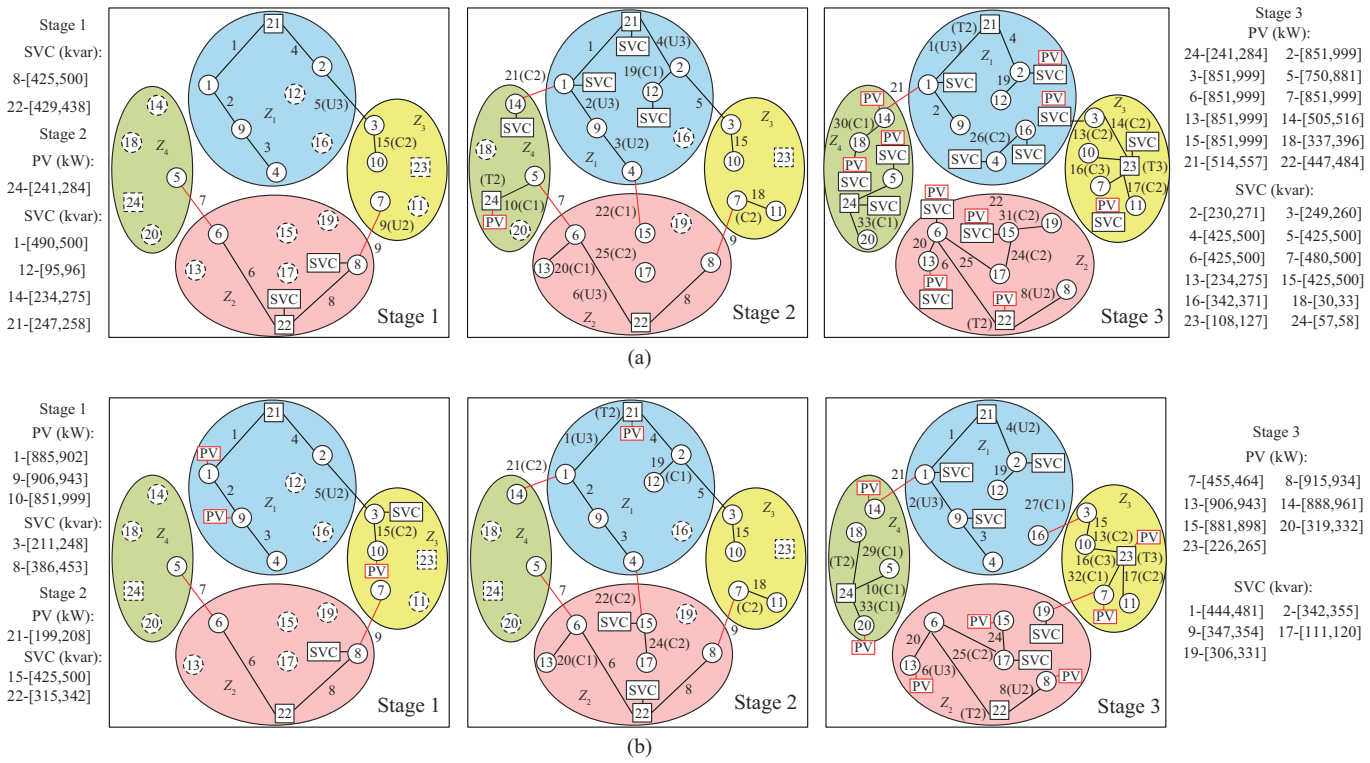

Fig. 4. Planning schemes of Pareto optimal solutions No. 2 and No. 8. (a) No. 2. (b) No. 8.

TABLE IV
INTERVAL VALUES OF $\hat{f}_1, f_2, \hat{f}_3, \hat{f}_4$, PV INSTALLATION CAPACITY, AND SVC COMPENSATION CAPACITY

No.	$\hat{f}_1$ (M$)	f_2 (%)	$\hat{f}_3$ (%)	$\hat{f}_4$ (%)	N_{PV}	$\hat{P}_{PV}^{cap}$ (kW)	N_{SVC}	$\hat{Q}_{SVC}$ (kvar)
1	[12.41,12.96]	18.11	[18.58,19.47]	[12.83,14.24]	15	[11188,12924]	14	[4213,4810]
2	[11.90,12.52]	19.57	[17.03,17.92]	[14.30,15.61]	12	[7900,9112]	18	[5350,5962]
3	[8.56,9.22]	18.38	[18.21,19.19]	[18.56,20.21]	10	[6827,7820]	13	[4914,5543]
4	[9.74,10.17]	22.13	[16.62,17.84]	[15.35,16.62]	11	[5104,5361]	15	[3884,4195]
5	[9.82,10.33]	19.53	[16.93,18.03]	[18.80,20.20]	10	[6955,7956]	16	[5164,5890]
6	[13.26,13.92]	13.17	[19.14,19.88]	[12.46,13.74]	16	[10775,12241]	18	[5913,6651]
7	[7.58,8.22]	17.62	[18.70,19.44]	[22.25,23.71]	9	[5831,6562]	8	[3337,3741]
8	[9.45,10.04]	31.90	[13.80,15.46]	[16.46,17.56]	11	[7431,7849]	9	[2887,3184]
9	[8.42,9.15]	16.47	[18.53,19.64]	[18.65,20.05]	9	[6889,7698]	17	[5484,6207]
10	[10.16,10.79]	26.02	[15.81,17.17]	[15.64,16.93]	11	[7145,8101]	16	[5283,6109]

TABLE V
INTERVAL VALUES OF COSTS AND PROFITS, TCD AND NCD, AND VOLTAGE AND CURRENT VIOLATION MARGINS

No.	$\hat{f}_{inv}$ (M$)	$\hat{f}_{o\&m}$ (M$)	f_{loss} (M$)	$\hat{f}_{pro}$ (M$)	D_{tcd} (%)	D_{ncd} (%)	$\hat{V}^{mar}$ (%)	$\hat{I}^{mar}$ (%)
1	[13.70,14.38]	[2.78,2.95]	[1.09,1.18]	[5.08,5.67]	19.50	16.73	[4.83,4.85]	[73.60,77.96]
2	[11.12,11.79]	[2.15,2.34]	[2.60,2.79]	[3.91,4.37]	15.08	24.06	[4.95,5.00]	[65.32,69.60]
3	[9.37,9.95]	[2.55,2.69]	[1.55,1.66]	[4.69,5.20]	13.77	23.00	[4.91,4.94]	[71.43,76.18]
4	[8.63,8.77]	[2.14,2.19]	[2.96,3.20]	[3.87,4.15]	13.99	30.27	[4.98,5.02]	[63.18,69.13]
5	[9.72,10.15]	[1.66,1.77]	[1.53,1.68]	[3.05,3.37]	19.44	19.62	[4.93,4.97]	[64.93,70.29]
6	[12.66,13.32]	[2.35,2.51]	[2.91,3.14]	[4.66,5.03]	13.08	13.27	[4.85,4.88]	[76.29,79.89]
7	[8.85,9.17]	[2.54,2.71]	[1.10,1.19]	[4.65,5.16]	15.65	19.58	[4.86,4.88]	[74.07,77.68]
8	[9.59,9.82]	[3.01,3.11]	[2.76,2.94]	[5.66,6.10]	22.78	41.02	[5.04,5.09]	[48.86,56.94]
9	[9.98,10.54]	[3.32,3.54]	[1.53,1.66]	[6.18,6.78]	13.30	19.64	[4.88,4.91]	[69.43,74.67]
10	[9.97,10.51]	[2.28,2.44]	[2.32,2.49]	[4.19,4.71]	19.64	32.41	[4.97,5.01]	[59.20,65.79]

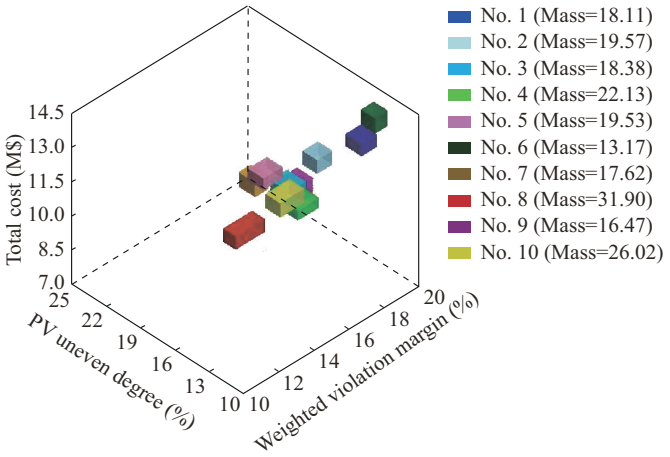

Fig. 5. AA-POF in multi-dimensional objective space.

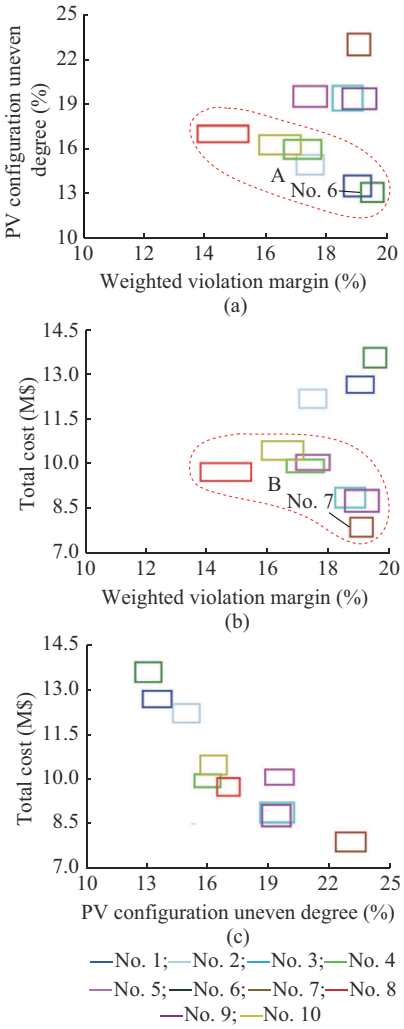

Fig. 6. Projections of AA-POF on different planes. (a) $\hat{f}_3$-$\hat{f}_4$ plane. (b) $\hat{f}_3$-$\hat{f}_1$ plane. (c) $\hat{f}_4$-$\hat{f}_1$ plane.

Therefore, the solutions No. 6 and No. 7 can still be regarded as bad solutions if $D_{\max}$ is set as 4 or less. And the modified AA-POF consists of eight feasible non-dominated solutions in total, which effectively improves the solution qualities.

TABLE VI
DEVIATION DISTANCES OF ALL PARETO OPTIMAL SOLUTIONS

k	$d_{AVG}(x_k)$	$O_{AVG}(x_k)$	V_{AVG}	$V(x_k)$	$D_{AVG}(x_k)$
1	7.0825	0	0.8747	0.6902	2.7613
2	4.4275	0	0.8747	0.7229	1.7045
3	4.5475	0	0.8747	1.0672	1.5458
4	2.3395	0	0.8747	0.6662	0.9206
5	3.0375	0.0005	0.8747	0.7854	1.1419
6	8.9075	0	0.8747	0.6252	3.5631
7	9.5025	0	0.8747	0.6915	3.7029
8	4.1245	0	0.8747	1.0956	1.3886
9	5.0025	0	0.8747	1.1242	1.6681
10	2.3475	0	0.8747	1.1053	0.7878

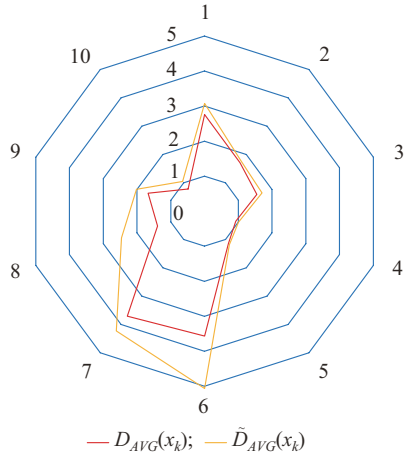

Fig. 7. Comparison of deviation distances $\tilde{D}_{AVG}(x_k)$ and $D_{AVG}(x_k)$.

$$\tilde{D}_{AVG}(x_k)=D_{AVG}(x_k)\cdot\exp\left(\left|\frac{f_2(x_k)}{f_{2,AVG}}-1\right|\right)\quad k=1,2,\ldots,10 \tag{51}$$

$$f_{2,AVG}=\frac{1}{10}\sum_{k=1}^{10}f_2(x_k) \tag{52}$$

C. Result Comparison

1) Different Uncertainty Levels

To quantify the influences of different uncertainty levels, the objectives $\hat{f}_1$, $\hat{f}_3$, and $\hat{f}_4$ of Pareto optimal solutions at the uncertainty levels of ±5%, ±10%, and ±20% are compared in Fig. 8. As can be observed, the interval range of each objective gets wider with the increase of uncertainty level. For the same objective, the interval variations of different solutions at three uncertainty levels are basically the same, while the variation characteristics for different objectives are diverse. Therefore, the selection of uncertainty level is important for the rationality of planning schemes. If the uncertainty level is set too high, the final interval will be too wide, which is of less reference significance. If the uncertainty level is too low, the interval will be too narrow, which cannot quantify the impacts of uncertainties. In reality, multiple planning objectives should be comprehensively considered to determine a reasonable uncertainty level.

2) Different Uncertainty Analysis Methods

To demonstrate the advantages of the AA-based planning method, the objectives $\hat{f}_1$, $\hat{f}_3$, and $\hat{f}_4$ of all ten Pareto optimal solutions obtained by the AA-, IA-, and MCS-based methods are compared in Fig. 9. As can be observed from Fig. 9, the simulation results of AA-based planning method are nearly close to the MCS-based method. This is because the AA-based planning method can keep track on the dependencies of multiple uncertain variables, so the computation conservativeness can be effectively reduced. In comparison, the IA-based method will obtain less accurate and conservative results for lacking the consideration of dependencies of various uncertain variables. Therefore, the AA-based method has great application values and advantages in the proposed bi-level multi-objective joint planning for its high computation accuracy and low conservativeness.

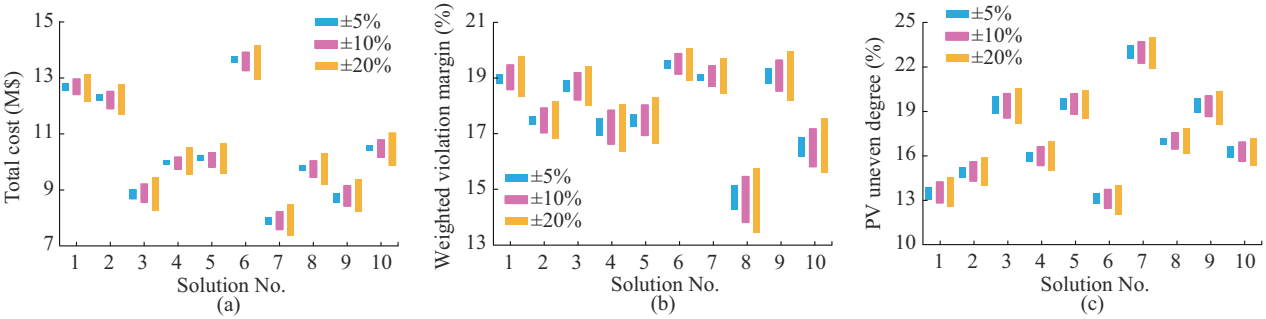

Fig. 8. Comparison of interval objective values under different uncertainty levels. (a) $\hat{f}_1$. (b) $\hat{f}_3$. (c) $\hat{f}_4$.

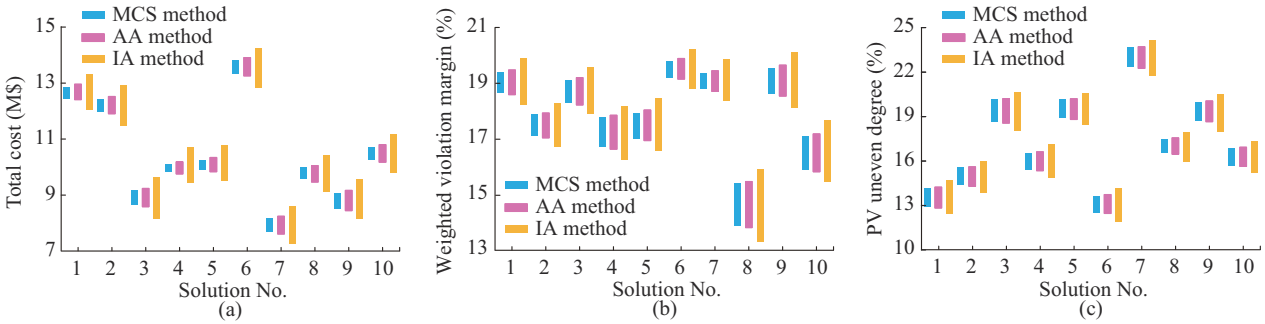

Fig. 9. Comparison of interval objective values by AA, IA, and MCS methods with uncertainty level of ±10%. (a) $\hat{f}_1$. (b) $\hat{f}_3$. (c) $\hat{f}_4$.

D. Test on Real Chinese 10 kV Distribution System

A real Chinese 10 kV distribution system shown in Fig. 10 is used for another case study to further validate the effectiveness of the proposed method. This system consists of 3 substation buses, 51 load buses, and 56 lines (including 5 tie-lines), which is divided into three geographical regions Z_1-Z_3. The whole planning horizon is divided into 2 stages, each lasting for 5 years. The data of peak load active power (power factor equals 0.9) and line length are shown in Table VII and Table VIII, respectively. The values of $P_{PV,i,h}^{cap,\max}$ and $Q_{SVC,i,h}^{\max}$ are set as 300 kW and 150 kvar, respectively. All other parameters are set the same as those of the 24-bus test system.

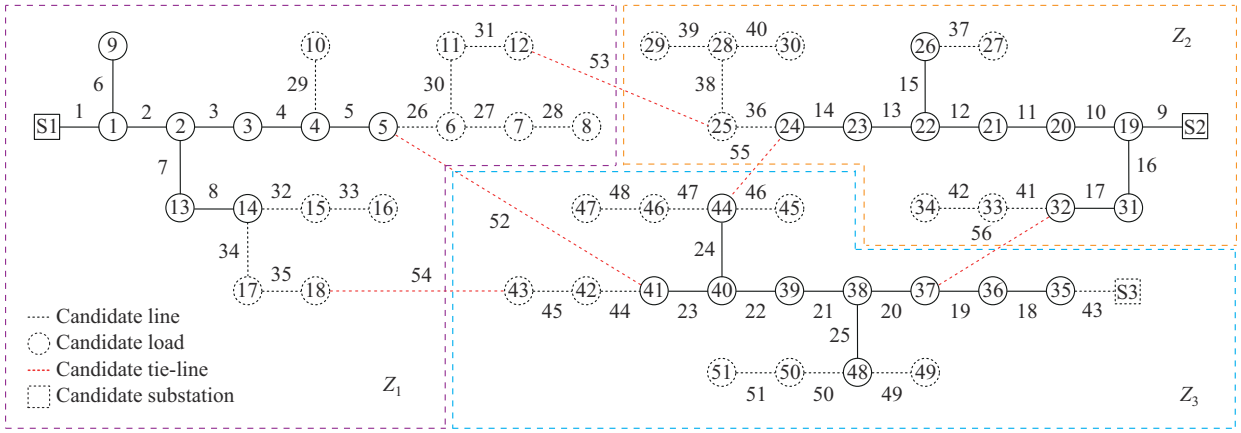

Fig. 10. Initial topology of real Chinese 10 kV distribution system.

TABLE VII
PEAK LOAD ACTIVE POWER OF CHINESE 10 KV DISTRIBUTION SYSTEM

Bus No.	Power (kW)		Bus No.	Power (kW)		Bus No.	Power (kW)	
	Stage 1	Stage 2		Stage 1	Stage 2		Stage 1	Stage 2
1	112	168	18	0	103	35	55	104
2	86	132	19	104	176	36	107	153
3	116	157	20	128	183	37	116	144
4	87	133	21	101	161	38	95	126
5	92	142	22	124	175	39	108	143
6	0	78	23	75	144	40	84	115
7	0	143	24	83	138	41	65	124
8	0	89	25	0	123	42	0	83
9	75	154	26	123	178	43	0	75
10	0	94	27	0	148	44	74	126
11	0	123	28	0	156	45	0	105
12	0	146	29	0	88	46	0	121
13	106	142	30	0	121	47	0	85
14	74	134	31	105	204	48	105	133
15	0	133	32	127	165	49	0	136
16	0	88	33	0	107	50	0	54
17	0	112	34	0	84	51	0	73

TABLE VIII
LINE LENGTH OF CHINESE 10 KV DISTRIBUTION SYSTEM

Line No.	l_{ij} (km)	Line No.	l_{ij} (km)	Line No.	l_{ij} (km)	Line No.	l_{ij} (km)
1	0.63	15	0.82	29	0.76	43	0.46
2	0.85	16	1.06	30	0.94	44	0.65
3	1.06	17	0.89	31	0.62	45	0.91
4	1.12	18	0.65	32	0.92	46	0.62
5	0.64	19	0.85	33	0.24	47	0.75
6	0.36	20	0.88	34	0.55	48	0.36
7	1.15	21	0.69	35	0.88	49	0.52
8	0.65	22	0.36	36	0.77	50	0.84
9	0.76	23	0.75	37	0.68	51	0.76
10	1.08	24	0.89	38	0.57	52	1.08
11	0.72	25	0.44	39	0.89	53	0.58
12	0.88	26	0.69	40	0.74	54	0.76
13	0.65	27	0.93	41	0.54	55	0.84
14	0.47	28	0.44	42	0.48	56	0.67

1) Bi-level Multi-objective Joint Planning

By using the AA-based dominance relation weakening criterion and bi-level multi-objective solution methodology, a total of five Pareto optimal solutions are obtained. The interval objective values of all Pareto optimal solutions are listed in Table IX and Table X. The planning scheme of Pareto optimal solution No. 1 is shown in Fig. 11.

As is observed from Table IX and Table X, solution No. 1 has the smallest $\hat{f}_1$ value and relatively large $\hat{f}_3$ value among five Pareto optimal solutions, while its f_2 and $\hat{f}_4$ objectives are poor. In comparison, solution No. 2 has the best $\hat{f}_3$ and $\hat{f}_4$ objectives while its $\hat{f}_1$ and f_2 objectives are the worst, which further validates the multi-objective mutual dominance characteristics. The five Pareto optimal solutions obtained represent the non-dominated optimal planning schemes that can simultaneously meet DN economy and adaptability goals considering uncertainties, which is of great significance for practical DN planning in uncertain environment.

TABLE IX
INTERVAL OBJECTIVE VALUES OF $\hat{f}_1, f_2, \hat{f}_3$, AND $\hat{f}_4$

No.	$\hat{f}_1$ (M$)	f_2 (%)	$\hat{f}_3$ (%)	$\hat{f}_4$ (%)
1	[4.96,5.11]	14.18	[17.59,18.08]	[7.49,7.61]
2	[6.54,6.73]	11.19	[18.28,18.65]	[5.61,5.66]
3	[6.47,6.67]	16.95	[16.99,17.56]	[5.78,5.80]
4	[5.10,5.36]	16.24	[17.12,17.55]	[6.80,6.87]
5	[5.61,5.78]	21.83	[15.47,16.12]	[6.53,6.57]

TABLE X
INTERVAL OBJECTIVE VALUES OF D_{tcd}, D_{ncd}, $\hat{V}^{mar}$, AND $\hat{I}^{mar}$

No.	D_{tcd} (%)	D_{ncd} (%)	$\hat{V}^{mar}$ (%)	$\hat{I}^{mar}$ (%)
1	6.65	21.71	[4.25,4.34]	[70.99,73.03]
2	6.86	15.51	[4.40,4.47]	[73.83,75.36]
3	5.64	28.25	[4.36,4.47]	[67.53,69.92]
4	6.86	25.61	[4.36,4.45]	[68.16,69.97]
5	8.67	34.99	[4.16,4.27]	[60.70,63.54]

On this basis, the deviation distances $D_{AVG}(x_k)$ and $\tilde{D}_{AVG}(x_k)$ of all Pareto optimal solutions are calculated as shown in Table XI. Obviously, solution No. 2 has relatively larger $\tilde{D}_{AVG}(x_k)$ compared with other solutions. If $D_{\max}$ is set as 4, solution No. 2 will be a bad solution and should be eliminated. In this way, the final AA-POF can be effectively modified and the solution qualities can be greatly improved.

2) Parameter Sensitivity Analysis

In the proposed model, the weight coefficients α_1 and α_2 can quantify the contribution degrees of TCD and NCD to the DN network structural adaptability. Meanwhile, α_3 and α_4 can quantify contribution degrees of voltage violation margin and current violation margin to the DN operational adaptability. The tuning of these key parameters has more or less impacts on the final planning schemes, so a parameter sensitivity analysis is conducted for the real Chinese 10 kV distribution system as follows.

1) Sensitivity of α_1 and α_2

Three scenarios are used to analyze the sensitivity of weight coefficients α_1 and α_2. Scenario 1 is when $\alpha_1=\alpha_2=0.5$. Scenario 2 is when $\alpha_1=0.8$ and $\alpha_2=0.2$. Scenario 3 is when $\alpha_1=0.3$ and $\alpha_2=0.7$. The number of final Pareto optimal solutions and average objective values in scenarios 1, 2, and 3 are compared in Table XII.

As can be observed from Table XII, the number of final Pareto optimal solutions K_{nd} in scenario 2 is smaller than those in scenarios 1 and 3. This is because there are obvious differences of NCD values between various solutions while the TCD values have little differences, which means the optimality of objective f_2 is more sensitive to the NCD variation.

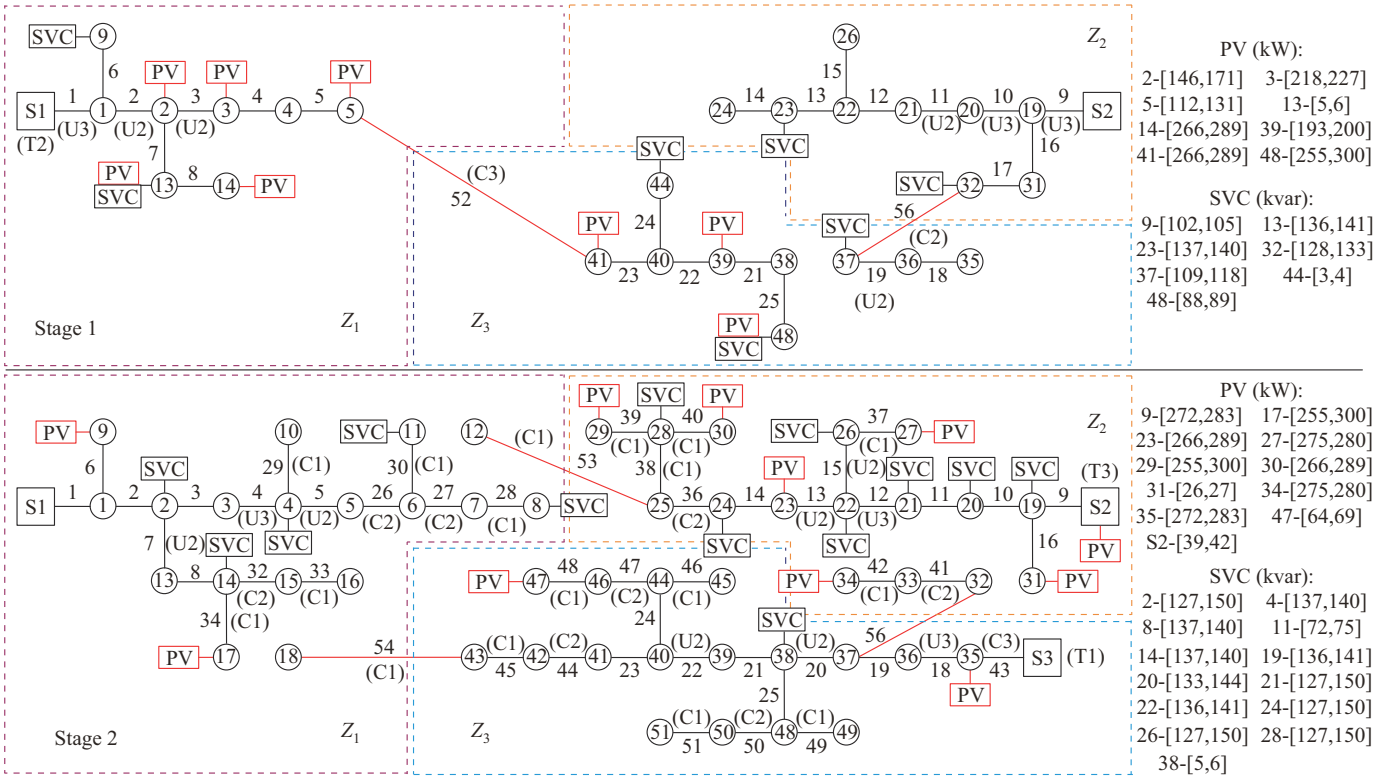

Fig. 11. Planning scheme of Pareto optimal solution No. 1.

TABLE XI
DEVIATION DISTANCES OF ALL PARETO OPTIMAL SOLUTIONS

k	$d_{AVG}(x_k)$	$O_{AVG}(x_k)$	V_{AVG}	$V(x_k)$	$D_{AVG}(x_k)$	$\tilde{D}_{AVG}(x_k)$
1	2.370	0	0.0058	0.0088	2.3359	2.6704
2	2.763	0	0.0058	0.0035	2.7375	4.2370
3	1.485	0	0.0058	0.0023	1.4731	1.5509
4	0.972	0	0.0058	0.0078	0.9590	0.9686
5	1.762	0	0.0058	0.0044	1.7442	2.2700

TABLE XII
COMPARISON OF PLANNING SCHEMES BETWEEN SCENARIOS 1, 2, AND 3

Scenario	K_{nd}	$\hat{f}_1^{avg}$ (M$)	f_2^{avg} (%)	$\hat{f}_3^{avg}$ (%)	$\hat{f}_4^{avg}$ (%)
1	5	[5.74,5.93]	16.08	[17.09,17.59]	[6.44,6.50]
2	4	[5.55,5.75]	10.70	[17.12,17.60]	[6.61,6.68]
3	5	[5.74,5.93]	19.73	[17.09,17.59]	[6.44,6.50]

In scenario 2 with small α_2 value, the objective f_2 of original Pareto optimal solution No. 3 has a significant decrease due to its large NCD value, which makes solution No. 3 dominated by other solutions. In comparison, all Pareto optimal solutions in scenario 3 can remain optimality due to a larger α_2 value than 0.5. Moreover, the objective f_2 presents obvious variation between different scenarios, while little change occurs for the other three objectives.

2) Sensitivity of α_3 and α_4

Three scenarios are used to analyze the sensitivity of weight coefficients α_3 and α_4. Scenario 1 is when $\alpha_3=0.8$ and $\alpha_4=0.2$. Scenario 4 is when $\alpha_3=\alpha_4=0.5$. Scenario 5 is when $\alpha_3=0.3$ and $\alpha_4=0.7$. The final planning schemes in three scenarios are compared in Table XIII. As can be observed from Table XIII, the value of K_{nd} in scenarios 1, 4, and 5 are the same. This is because the test system used is of small scale and power supply radius, which makes the voltage rise less obvious. In this condition, the optimality of objective $\hat{f}_3$ is more sensitive to the current violation margin $\hat{I}^{mar}$ rather than voltage violation margin $\hat{V}^{mar}$. In the whole solution space, the original five Pareto optimal solutions shown in Table X all have relatively large $\hat{I}^{mar}$ values compared with other solutions, so the increase of α_4 value will make their optimality stronger. Therefore, the number of final Pareto optimal solutions will remain unchanged.

TABLE XIII
COMPARISON OF PLANNING SCHEMES BETWEEN SCENARIOS 1, 4, AND 5

Scenario	K_{nd}	$\hat{f}_1^{avg}$ (M$)	f_2^{avg} (%)	$\hat{f}_3^{avg}$ (%)	$\hat{f}_4^{avg}$ (%)
1	5	[5.74,5.93]	16.08	[17.09,17.59]	[6.44,6.50]
4	5	[5.74,5.93]	16.08	[36.28,37.39]	[6.44,6.50]
5	5	[5.74,5.93]	16.08	[49.06,50.57]	[6.44,6.50]

V. CONCLUSION

In this paper, IA and AA are applied to quantify PV and load uncertainties, and an AA-based adaptability-oriented bi-level multi-objective joint planning model is built, which can obtain the planning schemes with low constraint violation risk, high reliability, and strong adaptability under uncertainties. On this basis, an AA-NSGA-II-based bi-level multi-objective solution methodology is proposed to calculate AA-POF. The obtained AA-POF represents a set of optimal plan-

ning schemes that can simultaneously meet DN economy and adaptability goals considering uncertainties, which is of great significance for practical DN planning in the complex uncertain environment. In addition, an AA-based dominance relation weakening criterion and a deviation distance based AA-POF modification method are proposed to eliminate bad solutions and improve the solution qualities. The simulation results in a modified 24-bus system show the multi-objective mutual dominance characteristics. The comparison of different uncertainty levels shows their diverse interval variations. The comparison of different methods demonstrates the advantages of proposed AA-based planning method for its high computation accuracy and low conservativeness. Moreover, the sensitivity analysis for a real Chinese 10 kV distribution system explores the impacts of key parameters on the final planning schemes.

REFERENCES

[1] F. Olivier, P. Aristidou, D. Ernst *et al*., "Active management of low-voltage networks for mitigating overvoltages due to photovoltaic units," *IEEE Transactions on Smart Grid*, vol. 7, no. 2, pp. 926-936, Mar. 2016.

[2] H. Wu, Y. Yuan, J. Zhu *et al*., "Potential assessment of spatial correlation to improve maximum distributed PV hosting capacity of distribution networks," *Journal of Modern Power Systems and Clean Energy*, vol. 9, no. 4, pp. 800-810, Jul. 2021.

[3] Y. Chai, L. Guo, C. Wang *et al*., "Network partition and voltage coordination control for distribution networks with high penetration of distributed PV units," *IEEE Transactions on Power Systems*, vol. 33, no. 3, pp. 3396-3407, May 2018.

[4] A. Kumar and P. Kumar, "Power quality improvement for grid-connected PV system based on distribution static compensator with fuzzy logic controller and UVT/ADALINE-based least mean square controller," *Journal of Modern Power Systems and Clean Energy*, vol. 9, no. 6, pp. 1289-1299, Nov. 2021.

[5] A. Luo, Q. Xu, F. Ma *et al*., "Overview of power quality analysis and control technology for the smart grid," *Journal of Modern Power Systems and Clean Energy*, vol. 4, no. 1, pp. 1-9, Jan. 2016.

[6] A. Keane, L. F. Ochoa, C. L. T. Borges *et al*., "State-of-the-art techniques and challenges ahead for distributed generation planning and optimization," *IEEE Transactions on Power Systems*, vol. 28, no. 2, pp. 1493-1502, May 2013.

[7] M. Nick, R. Cherkaoui, M. Paolone *et al*., "Optimal allocation of dispersed energy storage systems in active distribution networks for energy balance and grid support," *IEEE Transactions on Power Systems*, vol. 29, no. 5, pp. 2300-2310, Sept. 2014.

[8] G. Muñoz-Delgado, J. Contreras, and J. M. Arroyo, "Joint expansion planning of distributed generation and distribution networks," *IEEE Transactions on Power Systems*, vol. 30, no. 5, pp. 2579-2590, Sept. 2015.

[9] A. Tabares, J. F. Franco, M. Lavorato *et al*., "Multistage long-term expansion planning of electrical distribution systems considering multiple alternatives," *IEEE Transactions on Power Systems*, vol. 31, no. 3, pp. 1900-1914, May 2016.

[10] S. Jothibasu, A. Dubey, and S. Santoso, "Two-stage distribution circuit design framework for high levels of photovoltaic generation," *IEEE Transactions on Power Systems*, vol. 34, no. 6, pp. 5217-5226, Nov. 2019.

[11] Y. Fu and H. Chiang, "Toward optimal multiperiod network reconfiguration for increasing the hosting capacity of distribution networks," *IEEE Transactions on Power Delivery*, vol. 33, no. 5, pp. 2294-2304, Oct. 2018.

[12] N. N. Mansor and V. Levi, "Integrated planning of distribution networks considering utility planning concepts," *IEEE Transactions on Power Systems*, vol. 32, no. 6, pp. 4656-4672, Nov. 2017.

[13] Y. Li, W. Gao, W. Yan *et al*., "Data-driven optimal control strategy for virtual synchronous generator via deep reinforcement learning approach," *Journal of Modern Power Systems and Clean Energy*, vol. 9, no. 4, pp. 919-929, Jul. 2021.

[14] S. Sannigrahi, S. R. Ghatak, and P. Acharjee, "Multi-scenario based bi-level coordinated planning of active distribution system under uncertain environment," *IEEE Transactions on Industry Applications*, vol. 56, no. 1, pp. 850-863, Jan.-Feb. 2020.

[15] M. Jooshaki, H. Farzin, A. Abbaspour *et al*., "A model for stochastic planning of distribution network and autonomous DG units," *IEEE Transactions on Industrial Informatics*, vol. 16, no. 6, pp. 3685-3696, Jun. 2020.

[16] Y. Gao, X. Hu, W. Yang *et al*., "Multi-objective bilevel coordinated planning of distributed generation and distribution network frame based on multiscenario technique considering timing characteristics," *IEEE Transactions on Sustainable Energy*, vol. 8, no. 4, pp. 1415-1429, Oct. 2017.

[17] S. Wang, Y. Dong, L. Wu *et al*., "Interval overvoltage risk based PV hosting capacity evaluation considering PV and load uncertainties," *IEEE Transactions on Smart Grid*, vol. 11, no. 3, pp. 2709-2721, May 2020.

[18] S. He, H. Gao, H. Tian *et al.*, "A two-stage robust optimal allocation model of distributed generation considering capacity curve and real-time price based demand response," *Journal of Modern Power Systems and Clean Energy*, vol. 9, no. 1, pp. 114-127, Jan. 2021.

[19] S. Wang, S. Chen, L. Ge *et al*., "Distributed generation hosting capacity evaluation for distribution systems considering the robust optimal operation of OLTC and SVC," *IEEE Transactions on Sustainable Energy*, vol. 7, no. 3, pp. 1111-1123, Jul. 2016.

[20] X. Chen, W. Wu, B. Zhang *et al*., "Data-driven DG capacity assessment method for active distribution networks," *IEEE Transactions on Power Systems*, vol. 32, no. 5, pp. 3946-3957, Sept. 2017.

[21] C. Zhang, H. Chen, K. Shi *et al*., "An interval power flow analysis through optimizing-scenarios method," *IEEE Transactions on Smart Grid*, vol. 9, no. 5, pp. 5217-5226, Sept. 2018.

[22] S. Wang, L. Han, and L. Wu, "Uncertainty tracing of distributed generations via complex affine arithmetic based unbalanced three-phase power flow," *IEEE Transactions on Power Systems*, vol. 30, pp. 3053-3062, Nov. 2015.

[23] S. Wang, K. Wang, F. Teng *et al*., "An affine arithmetic-based multi-objective optimization method for energy storage systems operating in active distribution networks with uncertainties," *Applied Energy*, vol. 223, pp. 215-228, Apr. 2018.

[24] F. S. Seta, L. W. de Oliveira, and E. J. de Oliveira, "Comprehensive approach for distribution system planning with uncertainties," *IET Generation, Transmission & Distribution*, vol. 13, no. 24, pp. 5467-5477, Nov. 2019.

[25] L. W. De Oliveira, F. D. S. Seta, and E. J. De Oliveira, "Optimal reconfiguration of distribution systems with representation of uncertainties through interval analysis," *International Journal of Electrical Power & Energy Systems*, vol. 83, pp. 382-391, Dec. 2016.

[26] G. Manson, "Calculating frequency response functions for uncertain systems using complex affine analysis," *Journal of Sound & Vibration*, vol. 288, no. 3, pp. 487-521, Aug. 2005.

[27] K. Deb, A. Pratap, S. Agarwal *et al*., "A fast and elitist multiobjective genetic algorithm: NSGA-II," *IEEE Transactions on Evolutionary Computation*, vol. 6, no. 2, pp. 182-197, Apr. 2002.

Shouxiang Wang received the B.S. and M.S. degrees in electrical engineering from Shandong University of Technology, Jinan, China, in 1995 and 1998, respectively, and the Ph.D. degree in electrical engineering from Tianjin University, Tianjin, China, in 2001. He is currently a Professor with the School of Electrical and Information Engineering, and Deputy Director of Key Laboratory of Smart Grid of Ministry of Education, Tianjin University. His research interests include distributed generation, microgrid, and smart distribution system.

Yichao Dong received the B.S. degree in electrical engineering from Tianjin University, Tianjin, China, in 2015, where he is currently pursuing the Ph.D. degree with the School of Electrical and Information Engineering. His research interest includes evaluation and planning of smart distribution system.

Qianyu Zhao received the B.S. and M.S. degrees in electrical engineering and control science and engineering from Tiangong University, Tianjin, China, in 2012 and 2015, respectively, and the Ph.D. degree in electrical engineering from Tianjin University, Tianjin, China, in 2020. She is currently an Assistant Professor with the School of Electrical and Information Engineering, Tianjin University. Her research interests include planning, assessment of energy storage and distributed generation, and uncertainty analysis of distribution networks.

Xu Zhang received the B.S. degree in electronic information engineering from Jilin University, Changchun, China, in 2006, the M.S. degree in radio frequency communication from University of Southampton, Southampton, United Kingdom, in 2008, and the Ph.D. degree in optical communication engineering from Technical University of Denmark, Lyngby, Denmark, in 2012. He is currently a Senior Engineer with the State Grid Tianjin Electric Power Company, Tianjin, China. His research interests include information communication, big data, and the Internet of Things.